CrossMark

ORIGINAL PAPER

Glass Forming and Crystallization Behavior of $(Fe_{1-x-y}Co_xNi_y)_{72}Cr_{15}Zr_{10}W_3$ Alloys

W. Li[1] · Y. Z. Yang[1]

Abstract Metalloid-free $(Fe_{1-x-y}Co_xNi_y)_{72}Cr_{15}Zr_{10}W_3$ (x, y = 0, 0.25) alloys were synthesized by a rapid quenching technique at the surface velocity of the cooper roller of 40 m/s. Glass-forming ability, crystallization kinetics, and saturation magnetization of the amorphous ribbons were analyzed by XRD, differential scanning calorimetry, and VSM. Results show that only $(Fe_{0.5}Co_{0.25}Ni_{0.25})_{72}Cr_{15}Zr_{10}W_3$ has an amorphous structure with ΔT_x = 39 K. The saturation magnetization (M_s) is 49.2 emu/g, and coercivity (H_c) is as low as 5.0 A/m. The apparent activation energies of the alloys were calculated to be E_x (K) = 331.8 kJ/mol and E_p (K) = 255.5 kJ/mol, respectively, by using the Kissinger and Ozawa plot method. The high activation energy of crystallization implies that the atomic diffusion in the $(Fe_{0.5}Co_{0.25}Ni_{0.25})_{72}Cr_{15}Zr_{10}W_3$ alloy system is difficult, demonstrating that the obtained amorphous ribbon exhibits high thermal stability. With the increase of heating rates, the crystallization characteristic temperatures increase correspondingly. After annealing, the crystallization process of the amorphous ribbon was the eutectic crystallization method for the multi-crystalline precipitation.

Keywords Amorphous ribbon · Heating rate · Crystallization behavior · Activation energy · Annealing

✉ Y. Z. Yang
yangyzgdut@163.com

1 Faculty of Materials and Energy, Guangdong University of Technology, Guangzhou 510006, China

1 Introduction

As an important engineering material, Fe-based amorphous alloy has obvious cost advantages and wide application, which has been widely concerned and researched in recent decades. With further research, various Fe-based amorphous alloy systems with good glass formation ability have been developed. However, these alloys have a common defect, brittleness, which makes it a great limitation for structural materials. The ferromagnetic Fe-based amorphous can be generally classified into four systems: Fe-(Al, Ga)-(P, C, B, Si, Ge) [1–3], (Fe, Co, Ni)-TM-B (TM = Zr, Nb, Ta, Hf, Mo, Ti, V, W) [4, 5], Fe-Co-Ln-B [6, 7], and Fe-(Cr, Mn)-(Mo, Co)-(C, B)-(Er, Y) [8–10]. Throughout the four Fe-based amorphous systems, at least one or more metalloids such as B, Si, P, and C are found in the multi-component metallic glasses. The total amount of the metalloid atoms is more than 20 %. Research studies have shown that brittleness is closely related to the type, content, and distribution of metalloid elements [11, 12]. Nowadays, for the ferromagnetic elements, the amorphous alloys without metalloids mainly concentrated in the Ni-based, the same as the ferromagnetic elements of the Fe-based and Co-based amorphous alloys without metalloids is rarely reported. Therefore, as a supplement to the research of amorphous alloy, it is very significant to develop Fe-based amorphous alloy without metalloids. In this paper, FeCoNiCrZrW amorphous ribbons without metalloids were prepared by the optimization of the components. The crystallization kinetics of amorphous alloy ribbons were studied by a continuous heating method.

2 Experimental Procedure

Alloys with nominal composition $(Fe_{1-x-y}Co_xNi_y)_{72}Cr_{15}Zr_{10}W_3$ (x, y = 0, 0.25) were refining into master alloy under a Ti-gettered Ar atmosphere in a vacuum arc furnace. Each ingot was re-melted for four times to minimize the compositional inhomogeneity. Rapidly solidified ribbons with a thickness of 20~30 μm and a width of 1~2 mm were prepared by a rapid quenching technique (40 m/s linear speed) under a controlled argon gas atmosphere. The structures of the prepared ribbons were identified by X-ray diffraction (XRD) using Cu K$_\alpha$ radiation with an angle range of 20° ~90°. Glass transition and crystallization behaviors were evaluated using differential scanning calorimetry (DSC) under a nitrogen atmosphere. Curves were recorded at constant heating rates of 10, 20, 30, and 40 K/min in the temperature range from room temperature to 1073 K. The hysteresis loop of as-quenched ribbon was measured by a vibrating sample magnetometer at room temperature. Coercivity was determined by the soft magnetic dc B-H loop analyzer.

3 Results and Discussion

3.1 X-ray Diffraction Analysis

Figure 1 shows an example of the XRD pattern of as-quenched $(Fe_{1-x-y}Co_xNi_y)_{72}Cr_{15}Zr_{10}W_3$ (x, y = 0, 0.25) ribbons. The results indicate a trend of transition from crystalline to amorphous by the addition of Co and Ni. It is apparent that the crystallization phase of α-Fe, Fe-Cr, and Fe$_2$Zr occurred in the Fe$_{72}$Cr$_{15}$Zr$_{10}$W$_3$ alloy composition

without Ni and Co. When only Co was added to substitute for Fe, the intensity of crystalline phase decreased slightly. The Fe$_2$Zr phase disappeared, and the intensity of crystalline phase decreased significantly when Ni was added alone to replace Fe. However, the typical broad halo can be seen around $2\theta = 45°$ and no sharp Bragg peaks are observed when the same amount of Co and Ni was added to substitute for Fe. The broad halo patterns indicate that the $(Fe_{0.5}Co_{0.25}Ni_{0.25})_{72}Cr_{15}Zr_{10}W_3$ ribbon consists of a fully amorphous phase.

3.2 DSC Analysis

The DSC curves of as-quenched ribbon shows an obvious exothermic peak in the temperature range of 793~893 K (as shown in Fig. 2). With the increase of heating rates (β), the endothermic peak shifts to higher temperatures, indicating that the crystallization behavior of the $(Fe_{0.5}Co_{0.25}Ni_{0.25})_{72}Cr_{15}Zr_{10}W_3$ alloy has an obvious thermodynamic effect. The peak temperature (T_P) is high, and the heat flow of the exothermic peak is large when the value of β is increased.

Figure 3 shows the DSC curves obtained from $(Fe_{0.5}Co_{0.25}Ni_{0.25})_{72}Cr_{15}Zr_{10}W_3$ alloy at different heating rates. The values of characteristic temperatures (as shown in the inset of Fig. 3), such as glass transition temperature (T_g), onset crystallization temperature (T_x), crystallization peak temperature (T_p), and temperature intervals of supercooled liquid (ΔT_x) at different heating rates are listed in Table 1.

3.3 Crystallization Kinetics and Behavior

Amorphous alloys are metastable in thermodynamics. The free energy of the amorphous state is higher than that of
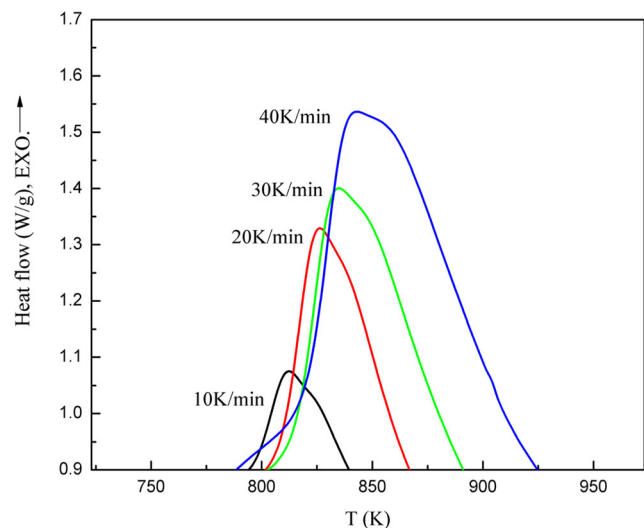

Fig. 1 XRD patterns of the $(Fe_{1-x-y}Co_xNi_y)_{72}Cr_{15}Zr_{10}W_3$ (x, y = 0, 0.25) alloy ribbons

Fig. 2 DSC curves of exothermic peak of the as-quenched $(Fe_{0.5}Co_{0.25}Ni_{0.25})_{72}Cr_{15}Zr_{10}W_3$ ribbons at different heating rates
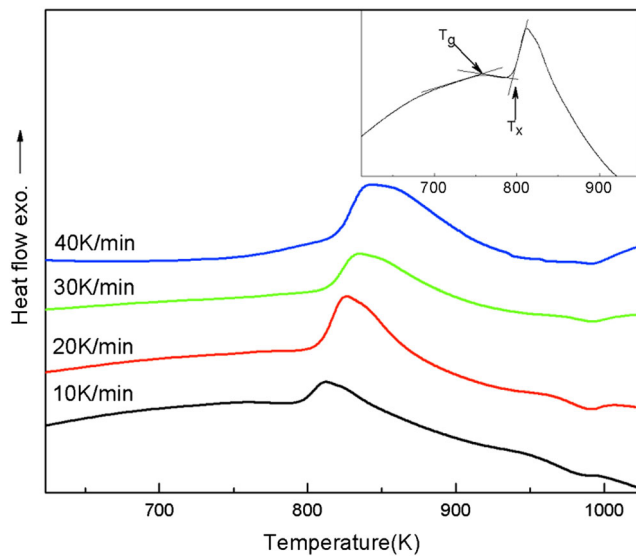
Fig. 3 DSC curves of $(Fe_{0.5}Co_{0.25}Ni_{0.25})_{72}Cr_{15}Zr_{10}W_3$ amorphous ribbons at different heating rates

the corresponding crystalline state. So, amorphous alloys are prone to crystallization under the conditions of heat or radiation. Studying the crystallization behavior from the perspective of thermodynamics is helpful to understand the crystallization mechanism of amorphous alloys. Crystallization activation energy (E), by nature, can reflect the energy needed to overcome the crystallization of amorphous alloys. It is the energy required that amorphous alloy transforms from the high stability of the glass state to the low stability of the glass state and crystalline state during heating. It represents the difficulty of glass transition and crystallization of amorphous alloys. In general, the higher the crystallization activation energy, the more stable the amorphous alloy in the liquid-phase region.

The apparent activation energy for crystallization process can be established by using the Kissinger plot method based on the following equation [13]:

$$\ln \frac{\beta}{T^2} = \frac{-E}{RT} + \text{const.} \tag{1}$$

where β represents the heating rate, T is the feature temperature, E is the apparent activation energy for crystallization,

Table 1 The characteristic temperatures of the $(Fe_{0.5}Co_{0.25}Ni_{0.25})_{72}Cr_{15}Zr_{10}W_3$ amorphous ribbon

Heating rate (K/min)	10	20	30	40
T_g	756	–	–	–
T_x	795	807	813	817
T_p	813	827	835	843
ΔT_x	39	–	–	–

and R is the gas constant. According to the characteristic temperature of samples at different heating rates (Table 1), the linear relationship between $\ln (\beta/T^2)$ and $1/T$ can be obtained based on (1). The slope indicates the value $-E/R$.

The apparent activation energy for crystallization process can also be calculated by the Ozawa equation [14]:

$$\ln \beta = \frac{-1.0516E}{RT} + \text{const.} \tag{2}$$

where the slope of $\ln \beta$ versus $1.0516/T$ reflects the value of $-E/R$, which can be obtained by plotting $\ln \beta$ versus $1/T$.

As illustrated in Fig. 4, the line with the slope of E_x and E_p can be obtained by straight linear fitting. The apparent activation energy for onset crystallization temperature (E_x (K)) and crystallization peak temperature (E_p (K)) are calculated to be E_x (K) = 331.8 kJ/mol and E_p (K) = 255.5 kJ/mol, respectively, by using the Kissinger equation. E can also be determined by the Ozawa equation (2), which gives the values of E_x (O) = 329.7 kJ/mol and E_p (O) = 246.9 kJ/mol, respectively. It is obvious that the apparent activation energy calculated from the Kissinger equation and Ozawa equation is very close. The result calculated by the Ozawa equation is slightly smaller than that calculated by the Kissinger equation. The crystallization activation energy of amorphous alloys such as Fe-, Zr-, Cu-, and Ti-based amorphous alloys is generally within the range of 200–400 kJ/mol [15–17]. The difficulty of crystallization for amorphous alloy is closely related to the apparent activation energy of crystallization. The greater the crystallization activation energy, the more difficult the crystallization process; on the contrary, the crystallization is more likely to occur. The high activation energy of crystallization indicates that the atomic diffusion in the $(Fe_{0.5}Co_{0.25}Ni_{0.25})_{72}Cr_{15}Zr_{10}W_3$ alloy system is difficult,

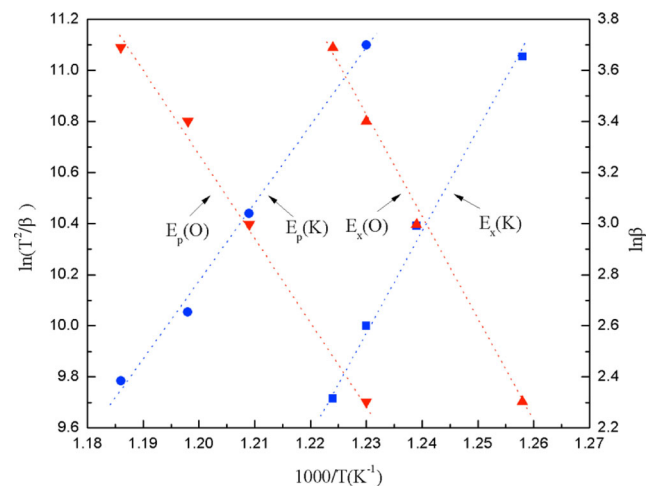**Fig. 4** Kissinger and Ozawa plots for the activation energy of the $(Fe_{0.5}Co_{0.25}Ni_{0.25})_{72}Cr_{15}Zr_{10}W_3$ amorphous alloy

demonstrating that the obtained amorphous ribbon exhibits high thermal stability [18].

Based on the DSC curves, the crystallized volume fraction (α) under non-isothermal crystallization conditions can be deduced by the following equations:

$$x = \frac{\Delta H_x}{\Delta H_o} = \frac{S_x}{S_o} \qquad (3)$$

where ΔH_α represents the total enthalpy of heat released during crystallization of amorphous alloys, ΔH_o is the sum of the enthalpy of heat released at a certain temperature (T) ($T_{on} \leq T \leq T_{end}$), S_α is the area between T_{on} and any given temperature (T), and S_o is the area ranging from T_{on} to T_{end} under the DSC curves, respectively. Figure 5 displays α plotted as a function of the temperature at different heating rates obtained from DSC curves according to relation in (3). From the graph, all curves show a sigmoid shape (S-type). It is obvious that each curve can be divided into three stages. For all of the heating rates, α/T in the initial and final stages of the curve is slow, but in the middle stage, α/T rises rapidly with the increase of temperature. This is because the early nucleation will be inoculated and nucleated everywhere in the amorphous matrix. Then, the grain grew rapidly in the early formation of the contact surface between the grains, and finally, the growing space for grain is decreased and disappeared eventually. With the increase of heating rate, the crystallization rate (α/T) decreased and the curves of α and T moved to the high-temperature region, which showed that the crystallization of $(Fe_{0.5}Co_{0.25}Ni_{0.25})_{72}Cr_{15}Zr_{10}W_3$ amorphous alloy had an obvious kinetic effect. That is, the faster the heating rate, the wider the crystallization temperature range.
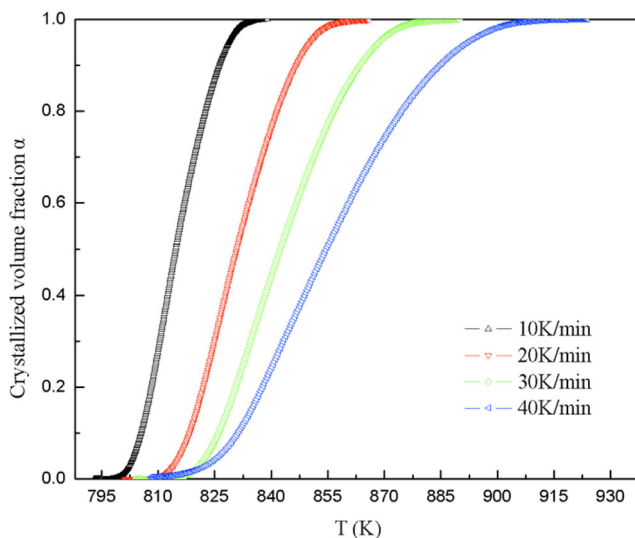
3.4 Saturation Magnetization (M_s) Analysis

The M-H loop of the as-quenched $(Fe_{0.5}Co_{0.25}Ni_{0.25})_{72}Cr_{15}Zr_{10}W_3$ ribbon is shown in Fig. 6. The value of saturation magnetization is 49.2 emu/g, while the coercive force is low of about 5.0 A/m. As can be seen, although the contents of the ferromagnetic elements (Fe, Co, and Ni) are relatively high, the M_s of the sample is low. This may be related to the dense random structure of the amorphous alloys with the addition of non-magnetic elements (Zr, Cr). However, the elements Zr and Cr is a key factor to improving the glass formation ability.

3.5 Alloy Stability and Crystallization Phase Formation

Figure 7 shows the XRD patterns of $(Fe_{0.5}Co_{0.25}Ni_{0.25})_{72}Cr_{15}Zr_{10}W_3$ ribbon annealed in a furnace at different temperatures for 10 min. The annealing temperature range from 743 to 873 K, based on the DSC test data with the heating rate of 10 K/min, and the samples were placed in the middle of the quartz tube of the furnace filled with the nitrogen to avoid oxidation. After annealing at 743 K, the amorphous structure of the sample did not significantly change. It is only able to note that the broad diffraction peak of the alloy becomes narrow. When the annealing temperature rose to 773 K, a sharp diffraction peak overlapping the broadened peak was identified to correspond to the precipitation of α-Fe(Co) phase in the amorphous matrix. However, when the alloys were annealed at 803 K, the α-Fe(Co) and Fe_2Zr phase was precipitated from the amorphous matrix simultaneously. Annealing the ribbons to 833 K led to an increase of α-Fe(Co) phase, which makes it more obvious of the corresponding crystallization diffraction peaks.
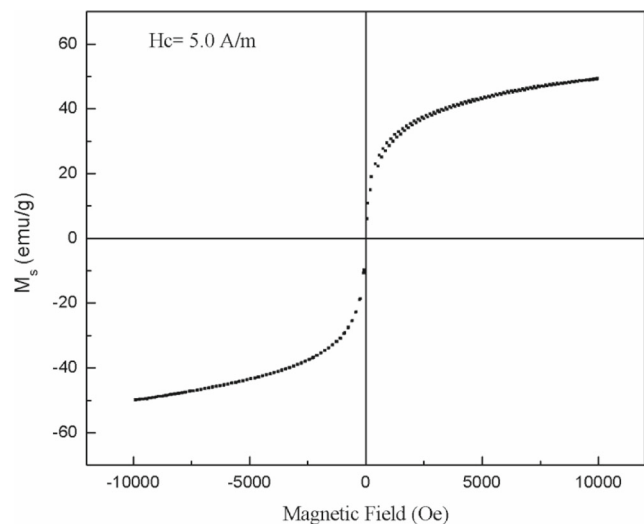

Fig. 5 Relationship between crystallized volume fraction and temperature at different heating rates for the $(Fe_{0.5}Co_{0.25}Ni_{0.25})_{72}Cr_{15}Zr_{10}W_3$ amorphous alloy

Fig. 6 Hysteresis loop of the $(Fe_{0.5}Co_{0.25}Ni_{0.25})_{72}Cr_{15}Zr_{10}W_3$ melt-spun ribbon
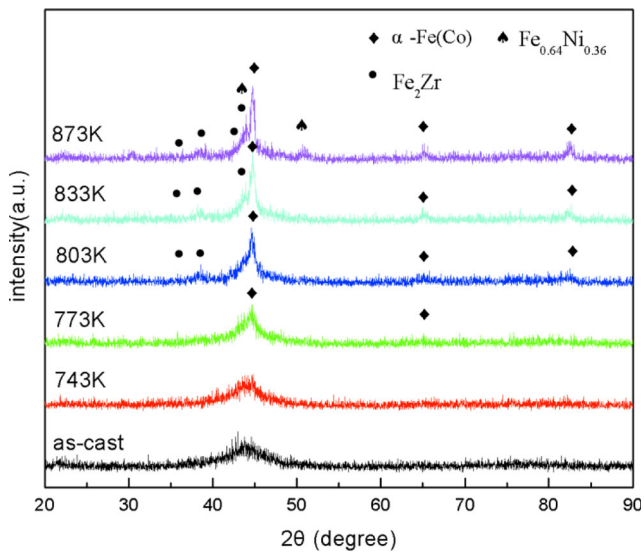
Fig. 7 XRD patterns of the $(Fe_{0.5}Co_{0.25}Ni_{0.25})_{72}Cr_{15}Zr_{10}W_3$ amorphous ribbon annealed at different temperatures

Further increasing the annealed temperature to 873 K, the disappearance of the broadened peak indicates the complete crystallization. It is clear that the relative intensity of crystallization peaks corresponding to α-Fe(Co) phase increases further, and the diffraction peaks corresponding to the $Fe_{0.64}Ni_{0.36}$ phase can be observed, implying more α-Fe(Co) and $Fe_{0.64}Ni_{0.36}$ phase precipitate.

4 Conclusion

1. The typical broad halo was only found in $(Fe_{0.5}Co_{0.25}Ni_{0.25})_{72}Cr_{15}Zr_{10}W_3$ alloy, implying its amorphous state. The apparent activation energy of onset crystallization temperature (E_x) and crystallization peak temperature (E_p) is determined as E_x (K) = 331.8 kJ/mol, E_x (O) = 329.7 kJ/mol, E_p (K) = 255.5 kJ/mol, and E_p (O) = 246.9 kJ/mol by the Kissinger and Ozawa equations, respectively. The apparent activation energy calculated from the Kissinger equation and Ozawa equation is very close. The high values of activation energy of crystallization indicate that the $(Fe_{0.5}Co_{0.25}Ni_{0.25})_{72}Cr_{15}Zr_{10}W_3$ amorphous alloy exhibits high thermal stability.
2. After heat treatment, the crystallization of the $(Fe_{0.5}Co_{0.25}Ni_{0.25})_{72}Cr_{15}Zr_{10}W_3$ amorphous ribbon is the eutectic crystallization method for the multicrystalline precipitation. When the annealing temperature reached 873 K, the precipitation of the crystallization phases contains α-Fe(Co), $Fe_{0.64}Ni_{0.36}$, and Fe_2Zr phase.

References

1. Inoue, A., Shinohara, Y., Gook, J.S.: Thermal magnetic properties of bulk Fe-based glassy alloys prepared by copper mold casting. Mater. Trans. JIM **36**(12), 1427–1433 (1995)
2. Inoue, A., Gook, J.S.: Effect of additional elements (M) on the thermal stability of supercooled liquid in $Fe_{72-x}Al_5Ga_2P_{11}C_6B_4M_x$ glassy alloys. Mater. Trans. JIM **37**(1), 32–38 (1996)
3. Wang, J., Cao, W., Wang, L., et al.: Fe–Al–P–C–B bulk metallic glass with good mechanical and soft magnetic properties. J. Alloys Comp. **637**, 5–9 (2015)
4. Inoue, A., Zhang, T., Itoi, T., et al.: New Fe-Co-Ni-Zr-B amorphous alloys with wide supercooled liquid regions and good soft magnetic properties. Mater. Trans. JIM **38**(4), 359–362 (1997)
5. Shen, T.D., Sun, B.R., Xin, S.W.: Influence of metalloids and annealing on the fundamental magnetic properties of bulk Fe–(Cr, Mo, Ga)–(P, B, C) metallic glasses. Intermetallics **65**, 111–116 (2015)
6. Zhang, W., Inoue, A.: Thermal magnetic properties of Fe-Co-Ln-B (Ln = Nd, Sm, Tb or Dy) amorphous alloys with high magnetostriction. Mater. Trans. JIM **40**(1), 78–81 (1999)
7. Imafuku, M., Yaoita, K., Sato, S., et al.: Local atomic structure of Fe-Co-Ln-B (Ln = Sm, Tb or Dy) amorphous alloys with supercooled liquid region. Mater. Sci. Eng. A **304**, 660–664 (2001)
8. Lu, Z.P., Liu, C.T., Thompson, J.R., et al: Structural amorphous steels. Phys. Rev. Lett. **92**(24), 245503 (2004)
9. Shen, J., Chen, Q., Sun, J., et al: Exceptionally high glass-forming ability of an FeCoCrMoCBY alloy. Applied Phys. Lett. **86**(15), 151907 (2005)
10. Han, J., Wang, C., Kou, S., et al.: Thermal stability, crystallization behavior, Vickers hardness and magnetic properties of Fe–Co–Ni–Cr–Mo–C–B–Y bulk metallic glasses. Trans. Nonferrous Metals Soc. China **23**(1), 148–155 (2013)
11. Zhang, T., Liu, F., Pang, S., et al.: Ductile Fe-based bulk metallic glass with good soft-magnetic properties. Mater. Trans. **48**(5), 1157–1160 (2007)
12. Jang, B.T., Kim, Y.I.: Effects of Cr or Mo compositions on mechanical behavior of Fe-base bulk amorphous alloy. Adv. Mater. Res. **1110**, 136–141 (2015)
13. Kissinger, H.E.: Variation of peak temperature with heating rate in differential thermal analysis. J. Res. Nat. Bureau Stand. **57**(4), 217–221 (1956)
14. Ozawa, T.: Kinetic analysis of derivative curves in thermal analysis. J. Thermal Anal. **2**(3), 301–324 (1970)
15. Pratap, A., Lad, K.N., Rao, T.L.S., et al.: Kinetics of crystallization of amorphous $Cu_{50}Ti_{50}$ alloy. J. Non-crystalline Solids **345**, 178–181 (2004)
16. Jang, J.S.C., Chen, Y.W., Chang, L.J., et al.: Crystallization and fracture behavior of the $Zr_{65x}Al_{7.5}Cu_{17.5}Ni_{10}Si_x$ bulk amorphous alloys. Mater. Chem. Phys. **89**(1), 122–129 (2005)
17. Xia, M.X., Ma, C.L., Zheng, H.X., et al.: Preparation and crystallization of $Ti_{53}Cu_{27} Ni_{12}Zr_3Al_7Si_3B_1$ bulk metallic glass with wide supercooled liquid region. Mater. Sci. Eng. A **390**(1), 372–375 (2005)
18. Movahedi, B., Enayati, M.H., Wong, C.C.: On the crystallization behavior of amorphous FeCrMoBPSi-C powder prepared by mechanical alloying. Mater. Lett. **64**(9), 1055–1058 (2010)